VII International Conference on Computational Methods for Coupled Problems in Science and Engineering
COUPLED PROBLEMS 2017
M. Papadrakakis, E. Oñate and B. Schrefler (Eds)

MIXED VARIATIONAL FORMULATIONS FOR MULTI-FIELD PROBLEMS

M. DITTMANN* AND C. HESCH*

* Chair of Computational Mechanics
University of Siegen
Paul-Bonatz-Straße 9-11, 57068 Siegen, Germany
e-mail: maik.dittmann@uni-siegen.de, christian.hesch@uni-siegen.de,
web page: https://www.mb.uni-siegen.de/nm/mitglieder/

Key words: Thermomechanical coupled problems, Polyconvex formulations, Hellinger-Reissner type variational principle

Abstract. The present work deals with large strain thermomechanical coupled problems. In particular, a novel polyconvex formulation based on a mixed Hellinger-Reissner type variational principle is introduced along with advanced discretization techniques which reduce the computational effort dramatically. Eventually, the capabilities of the proposed framework are demonstrated within a number of numerical examples.

1 INTRODUCTION

General thermoelastic material models have been investigated over the past decades, see e.g. Reese and Govindjee [1], Holzapfel and Simo [2] and Miehe [3] among many others. In this paper we present a novel computational framework for large strain thermoelasticity. The ideas of a new formulation for polyconvex large strain elasticity originally introduced by Ball [4] and recently resumed by Bonet et al. [5] are extended to non-linear coupled thermoelasticity, see also Dittmann [6]. In particular, the deformation gradient (line map), its co-factor (area map) and its determinant (volume map) along with the absolute temperature are formulated as independent variables to obtain a polyconvex free energy function. Moreover, we introduce work conjugate stresses to the extended kinematic set to define a complementary energy principle of Hellinger-Reissner type, where the introduced conjugate stresses along with the deformed geometry and the absolute temperature constitute the set of primal variables, see also Hesch et al. [7] for the application of a mixed Hu-Washizu type variational principle in the context of coupled phase-field fracture problems. The finite element discretization relies on a quadratic approximation of the deformed geometry and the absolute temperature, whereas discontinuous linear interpolations are used for the conjugate stresses such that the stress unknowns can be

condensed. Eventually, quasi-static as well as transient numerical examples are investigated to demonstrate the capability of the proposed framework.

2 CONFIGURATION AND KINEMATICS

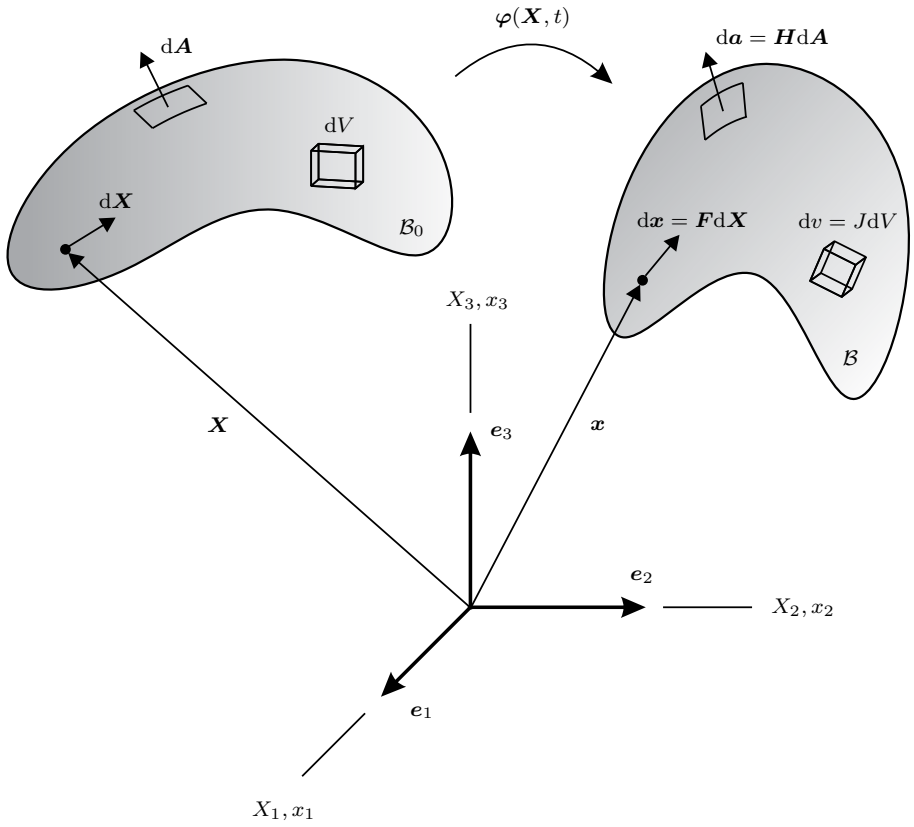

Figure 1: Deformation mapping of a continuum body from a reference configuration $\mathcal{B}_0$ into a current configuration $\mathcal{B}$ and associated strain measures $\boldsymbol{F}, \boldsymbol{H}$ and J

We consider a three dimensional thermoelastic body, i.e. $d = 3$, in its reference configuration occupying a domain $\mathcal{B}_0$ with boundary $\partial\mathcal{B}_0$, see Figure 1. A sufficiently smooth non-linear deformation mapping

$$\boldsymbol{\varphi}(\boldsymbol{X},t) : \mathcal{B}_0 \times \mathcal{T} \to \mathbb{R}^d, \tag{1}$$

is introduced to map a material point $\boldsymbol{X}$ in its reference configuration to its position $\boldsymbol{x} = \boldsymbol{\varphi}(\boldsymbol{X},t)$ in the current configuration $\mathcal{B}$ at time $t \in \mathcal{T} = [0,T]$, where $T \in \mathbb{R}^+$. Furthermore, we introduce the absolute temperature

$$\theta(\boldsymbol{X},t) : \mathcal{B}_0 \times \mathcal{T} \to \mathbb{R}_{\geq 0}, \tag{2}$$

which is assumed to be a sufficiently smooth function. The unknowns $\{\boldsymbol{\varphi}, \theta\}$ represent the non-reducible degrees of freedom to be found for all times of interest.

The deformation gradient tensor $\boldsymbol{F} : \mathcal{B}_0 \times \mathcal{T} \to \mathbb{R}^{d\times d}$ is commonly defined as material gradient of the current configuration

$$\boldsymbol{F} = \nabla(\boldsymbol{\varphi}) = \frac{\partial \boldsymbol{\varphi}}{\partial \boldsymbol{X}}. \tag{3}$$

Moreover, we introduce the determinant $J : \mathcal{B}_0 \times \mathcal{T} \to \mathbb{R}$ as well as the co-factor $\boldsymbol{H} : \mathcal{B}_0 \times \mathcal{T} \to \mathbb{R}^{d\times d}$ of the deformation gradient, usually defined by $J = \det(\boldsymbol{F})$ and $\boldsymbol{H} = J\boldsymbol{F}^{-1}$, respectively. As shown in Figure 1, the three strain measures $\boldsymbol{F}, \boldsymbol{H}$ and J map differential line, area and volume elements between the reference and the current configuration, i.e. $\mathrm{d}\boldsymbol{x} = \boldsymbol{F}\mathrm{d}\boldsymbol{X}$, $\mathrm{d}\boldsymbol{a} = \boldsymbol{H}\mathrm{d}\boldsymbol{A}$ and $\mathrm{d}v = J\mathrm{d}V$. Regarding the latter both mappings, we provide an alternative representation by using the cross product between second order tensors[1]. Thus, the co-factor or area map tensor is given as

$$\boldsymbol{H} = \mathrm{cof}(\boldsymbol{F}) = \frac{1}{2}(\boldsymbol{F} \times \boldsymbol{F}) \tag{4}$$

and the Jacobian determinant or volume map reads

$$J = \det(\boldsymbol{F}) = \frac{1}{6}(\boldsymbol{F} \times \boldsymbol{F}) : \boldsymbol{F}. \tag{5}$$

Note that the tensor cross product operation was originally introduced by de Boer [8] and for the first time applied in the context of solid mechanics in Bonet et al. [5]. The usage of the tensor cross product operation simplifies tremendously the first and second directional derivatives of (4) and (5) with respect to virtual and incremental variations $\delta\boldsymbol{\varphi}$ and $\Delta\boldsymbol{\varphi}$, since differentiation of the inverse of the deformation gradient is not required. For the co-factor follows immediately

$$\mathrm{D}\boldsymbol{H}[\delta\boldsymbol{\varphi}] = \boldsymbol{F} \times \nabla(\delta\boldsymbol{\varphi}), \quad \mathrm{D}^2\boldsymbol{H}[\delta\boldsymbol{\varphi}, \Delta\boldsymbol{\varphi}] = \nabla(\delta\boldsymbol{\varphi}) \times \nabla(\Delta\boldsymbol{\varphi}), \tag{6}$$

whereas the derivatives of the determinant of the deformation gradient read

$$\mathrm{D}J[\delta\boldsymbol{\varphi}] = \boldsymbol{H} : \nabla(\delta\boldsymbol{\varphi}), \quad \mathrm{D}^2J[\delta\boldsymbol{\varphi}, \Delta\boldsymbol{\varphi}] = \boldsymbol{F} : (\nabla(\delta\boldsymbol{\varphi}) \times \nabla(\Delta\boldsymbol{\varphi})). \tag{7}$$

3 POLYCONVEX THERMOELASTICITY

Polyconvexity is accepted as a fundamental mathematical requirement which has to be satisfied by admissible energy density functions to model large strain elastic material behavior.

[1]The definition of the tensor cross product operation is given e.g. in Dittmann [6], Appendix A.

3.1 Free Helmholtz energy

For the consideration of thermomechanical materials, the free Helmholtz energy density can be defined as a polyconvex function[2] of the introduced set of strains and the absolute temperature

$$\Psi(\boldsymbol{F},\theta) := \bar{\Psi}(\bar{\boldsymbol{F}},\bar{\boldsymbol{H}},J,\theta), \tag{8}$$

where the isochoric components of $\boldsymbol{F}$ and $\boldsymbol{H}$ are given as

$$\bar{\boldsymbol{F}} = J^{-1/3}\boldsymbol{F}, \quad \bar{\boldsymbol{H}} = J^{-2/3}\boldsymbol{H}. \tag{9}$$

Thus, a typical thermoelastic compressible Mooney-Rivlin material can be described by the free Helmholtz energy density function

$$\begin{aligned}\bar{\Psi}(\bar{\boldsymbol{F}},\bar{\boldsymbol{H}},J,\theta) = &\underbrace{\alpha(\bar{\boldsymbol{F}}:\bar{\boldsymbol{F}}-d)+\beta((\bar{\boldsymbol{H}}:\bar{\boldsymbol{H}})^{3/2}-d^{3/2})}_{\bar{\Psi}^{\mathrm{iso}}}+\underbrace{\frac{\kappa}{2}(J-1)^2}_{\bar{\Psi}^{\mathrm{vol}}}\\ &+\underbrace{c\left(\theta-\theta_{\mathrm{ref}}-\theta\ln\left(\frac{\theta}{\theta_{\mathrm{ref}}}\right)\right)}_{\bar{\Psi}^{\mathrm{the}}}+\underbrace{(-d\gamma(\theta-\theta_{\mathrm{ref}})\kappa(J-1))}_{\bar{\Psi}^{\mathrm{cpl}}},\end{aligned} \tag{10}$$

where α and β are positive material parameters related to the shear modulus and κ is the positive bulk modulus. Furthermore, the thermal material parameters $c \geq 0$ and γ denote the specific heat capacity and the linear thermal expansion coefficient, respectively. For more details and a proof of polyconvexity see Dittmann [6] and the references therein.

3.2 Conjugate stresses, entropy and Hessian operator

We introduce a set of work conjugate variables to the extended kinematic set and the temperature $\{\boldsymbol{F},\boldsymbol{H},J,\theta\}$ defined as

$$\boldsymbol{\Sigma}_F = \frac{\partial\bar{\Psi}}{\partial\boldsymbol{F}}, \quad \boldsymbol{\Sigma}_H = \frac{\partial\bar{\Psi}}{\partial\boldsymbol{H}}, \quad \Sigma_J = \frac{\partial\bar{\Psi}}{\partial J}, \quad \eta = -\frac{\partial\bar{\Psi}}{\partial\theta}. \tag{11}$$

In addition, work conjugate stresses to the isochoric strain components $\{\bar{\boldsymbol{F}},\bar{\boldsymbol{H}}\}$ can be formulated as

$$\bar{\boldsymbol{\Sigma}}_F = \frac{\partial\bar{\Psi}^{\mathrm{iso}}}{\partial\bar{\boldsymbol{F}}}, \quad \bar{\boldsymbol{\Sigma}}_H = \frac{\partial\bar{\Psi}^{\mathrm{iso}}}{\partial\bar{\boldsymbol{H}}}. \tag{12}$$

Accordingly, the hydrostatic pressure work conjugate to J is given as

$$p = \frac{\partial(\bar{\Psi}^{\mathrm{vol}}+\bar{\Psi}^{\mathrm{cpl}})}{\partial J} \tag{13}$$

and is positive in tension and negative in compression.

[2]Note that polyconvexity is related to the set of strains independent of the temperature field.

Next, we derive the relationship between the first Piola-Kirchhoff stress tensor $\boldsymbol{P}$ and the introduced sets of stresses $\{\boldsymbol{\Sigma}_F, \boldsymbol{\Sigma}_H, \Sigma_J\}$ and $\{\bar{\boldsymbol{\Sigma}}_F \bar{\boldsymbol{\Sigma}}_H, p\}$, respectively. The variation of both energy functions in (8) with respect to the primal variables formally reads

$$\mathrm{D}\Psi[\mathrm{D}\boldsymbol{F}[\delta\boldsymbol{\varphi}], \delta\theta] = \mathrm{D}\bar{\Psi}[\mathrm{D}\boldsymbol{F}[\delta\boldsymbol{\varphi}], \mathrm{D}\boldsymbol{H}[\delta\boldsymbol{\varphi}], \mathrm{D}J[\delta\boldsymbol{\varphi}], \delta\theta]. \tag{14}$$

Recalling (6) and (7) yields

$$\begin{aligned} \boldsymbol{P} : \nabla(\delta\boldsymbol{\varphi}) - \eta\delta\theta &= \boldsymbol{\Sigma}_{\boldsymbol{F}} : \mathrm{D}\boldsymbol{F}[\delta\boldsymbol{\varphi}] + \boldsymbol{\Sigma}_{\boldsymbol{H}} : \mathrm{D}\boldsymbol{H}[\delta\boldsymbol{\varphi}] + \Sigma_J \mathrm{D}J[\delta\boldsymbol{\varphi}] - \eta\delta\theta \\ &= (\boldsymbol{\Sigma}_{\boldsymbol{F}} + \boldsymbol{\Sigma}_{\boldsymbol{H}} \times \boldsymbol{F} + \Sigma_J \boldsymbol{H}) : \nabla(\delta\boldsymbol{\varphi}) - \eta\delta\theta. \end{aligned} \tag{15}$$

Thus, we find that

$$\begin{aligned} \boldsymbol{P} &= \boldsymbol{\Sigma}_F + \boldsymbol{\Sigma}_H \times \boldsymbol{F} + \Sigma_J \boldsymbol{H} \\ &= J^{-1/3}\bar{\boldsymbol{\Sigma}}_F + J^{-2/3}\bar{\boldsymbol{\Sigma}}_H \times \boldsymbol{F} + \left(p - \frac{1}{3} J^{-4/3} \bar{\boldsymbol{\Sigma}}_F : \boldsymbol{F} - \frac{2}{3} J^{-5/3} \bar{\boldsymbol{\Sigma}}_H : \boldsymbol{H} \right) \boldsymbol{H}. \end{aligned} \tag{16}$$

For the Newton-Raphson iteration a linearization is required. Regarding (15), the linearization reads

$$\begin{aligned} \mathrm{D}^2\bar{\Psi}[\delta\boldsymbol{\varphi}, \delta\theta, \Delta\boldsymbol{\varphi}, \Delta\theta] &= \begin{bmatrix} \nabla(\delta\boldsymbol{\varphi}) : & \delta\theta \end{bmatrix} \begin{bmatrix} \mathrm{D}\boldsymbol{P}[\nabla(\Delta\boldsymbol{\varphi}), \Delta\theta] \\ -\mathrm{D}\eta[\nabla(\Delta\boldsymbol{\varphi}), \Delta\theta] \end{bmatrix} \\ &= \begin{bmatrix} \nabla(\delta\boldsymbol{\varphi}) : \\ \nabla(\delta\boldsymbol{\varphi}) \times \boldsymbol{F} : \\ \nabla(\delta\boldsymbol{\varphi}) : \boldsymbol{H} \\ \delta\theta \end{bmatrix}^{\mathrm{T}} [\mathbb{H}_{\bar{\Psi}}] \begin{bmatrix} : \nabla(\Delta\boldsymbol{\varphi}) \\ : \nabla(\Delta\boldsymbol{\varphi}) \times \boldsymbol{F} \\ \nabla(\Delta\boldsymbol{\varphi}) : \boldsymbol{H} \\ \Delta\theta \end{bmatrix} \\ &\quad + (\boldsymbol{\Sigma}_{\boldsymbol{H}} + \Sigma_J \boldsymbol{F}) : (\nabla(\delta\boldsymbol{\varphi}) \times \nabla(\Delta\boldsymbol{\varphi})), \end{aligned} \tag{17}$$

where the Hessian operator is defined as

$$[\mathbb{H}_{\bar{\Psi}}] = \begin{bmatrix} \frac{\partial^2\bar{\Psi}}{\partial\boldsymbol{F}\partial\boldsymbol{F}} & \frac{\partial^2\bar{\Psi}}{\partial\boldsymbol{F}\partial\boldsymbol{H}} & \frac{\partial^2\bar{\Psi}}{\partial\boldsymbol{F}\partial J} & \frac{\partial^2\bar{\Psi}}{\partial\boldsymbol{F}\partial\theta} \\ \frac{\partial^2\bar{\Psi}}{\partial\boldsymbol{H}\partial\boldsymbol{F}} & \frac{\partial^2\bar{\Psi}}{\partial\boldsymbol{H}\partial\boldsymbol{H}} & \frac{\partial^2\bar{\Psi}}{\partial\boldsymbol{H}\partial J} & \frac{\partial^2\bar{\Psi}}{\partial\boldsymbol{H}\partial\theta} \\ \frac{\partial^2\bar{\Psi}}{\partial J\partial\boldsymbol{F}} & \frac{\partial^2\bar{\Psi}}{\partial J\partial\boldsymbol{H}} & \frac{\partial^2\bar{\Psi}}{\partial J\partial J} & \frac{\partial^2\bar{\Psi}}{\partial J\partial\theta} \\ \frac{\partial^2\bar{\Psi}}{\partial\theta\partial\boldsymbol{F}} & \frac{\partial^2\bar{\Psi}}{\partial\theta\partial\boldsymbol{H}} & \frac{\partial^2\bar{\Psi}}{\partial\theta\partial J} & \frac{\partial^2\bar{\Psi}}{\partial\theta\partial\theta} \end{bmatrix}. \tag{18}$$

The first term in $(17)_2$ represents the material part of the linearization, whereas the geometrical part is given via the second term. As shown in Bonet et al. [5], geometrical effects like buckling are solely expressed by the latter term.

3.3 Complementary energy

Assuming that the relationship between the work conjugate variables $\{\bar{\boldsymbol{F}}, \bar{\boldsymbol{H}}, J\}$ and $\{\bar{\boldsymbol{\Sigma}}_{\boldsymbol{F}}, \bar{\boldsymbol{\Sigma}}_{\boldsymbol{H}}, p\}$ is invertible, we define a complementary energy density function by means of the Legendre transformation

$$\bar{\Upsilon}(\bar{\boldsymbol{\Sigma}}_F, \bar{\boldsymbol{\Sigma}}_H, p, \theta) = \sup_{\bar{\boldsymbol{F}}, \bar{\boldsymbol{H}}, J} \{\bar{\boldsymbol{\Sigma}}_F : \bar{\boldsymbol{F}} + \bar{\boldsymbol{\Sigma}}_H : \bar{\boldsymbol{H}} + pJ - \bar{\Psi}(\bar{\boldsymbol{F}}, \bar{\boldsymbol{H}}, J, \theta)\}. \tag{19}$$

Regarding (10), this leads to

$$\begin{aligned}\bar{\Upsilon} &= \bar{\boldsymbol{\Sigma}}_F : \bar{\boldsymbol{F}}(\bar{\boldsymbol{\Sigma}}_F) + \bar{\boldsymbol{\Sigma}}_H : \bar{\boldsymbol{H}}(\bar{\boldsymbol{\Sigma}}_H) + pJ(p,\theta) - \Psi(\bar{\boldsymbol{F}}(\bar{\boldsymbol{\Sigma}}_F), \bar{\boldsymbol{H}}(\bar{\boldsymbol{\Sigma}}_H), J(p,\theta), \theta) \\ &= \frac{1}{4\alpha}\bar{\boldsymbol{\Sigma}}_F : \bar{\boldsymbol{\Sigma}}_F + \alpha d + \frac{2}{3\sqrt{3\beta}}(\bar{\boldsymbol{\Sigma}}_H : \bar{\boldsymbol{\Sigma}}_H)^{3/4} + \beta d^{3/2} + \frac{1}{2\kappa}p^2 + p + d\gamma(\theta - \theta_{\mathrm{ref}})p \\ &\quad - c\left(\theta - \theta_{\mathrm{ref}} - \theta \ln\left(\frac{\theta}{\theta_{\mathrm{ref}}}\right)\right) + \frac{\kappa}{2}(d\gamma(\theta - \theta_{\mathrm{ref}}))^2,\end{aligned} \tag{20}$$

where expressions for $\bar{\boldsymbol{F}}(\bar{\boldsymbol{\Sigma}}_F)$, $\bar{\boldsymbol{H}}(\bar{\boldsymbol{\Sigma}}_H)$ and $J(p,\theta)$ may deduced directly by inverting the relations obtained with (12) and (13).

4 VARIATIONAL FORMULATION

In the sense of a Hellinger-Reissner type variational principle, the original set of unknowns is extended by the stress fields. Accordingly, we define $\{\boldsymbol{\varphi}, \theta, \bar{\boldsymbol{\Sigma}}_F^*, \bar{\boldsymbol{\Sigma}}_H^*, p^*\}$ as extended set of independent variables[3]. Next, we perform two consecutive Legendre transformations

$$\begin{aligned}e(\boldsymbol{F}, \eta) &= \bar{\Psi}(\bar{\boldsymbol{F}}, \bar{\boldsymbol{H}}, J, \theta) + \theta\eta \\ &= -\bar{\Upsilon}(\bar{\boldsymbol{\Sigma}}_F^*, \bar{\boldsymbol{\Sigma}}_H^*, p^*, \theta) + \bar{\boldsymbol{\Sigma}}_F^* : \bar{\boldsymbol{F}} + \bar{\boldsymbol{\Sigma}}_H^* : \bar{\boldsymbol{H}} + p^* J + \theta\eta\end{aligned} \tag{21}$$

and state the global energy balance in terms of the complementary energy density function as follows

$$\begin{aligned}\int_{\mathcal{B}_0} \Bigg(&(\dot{\boldsymbol{\pi}} - \mathrm{Div}(\boldsymbol{P}) - \boldsymbol{B}) \cdot \dot{\boldsymbol{\varphi}} + \left(\bar{\boldsymbol{F}} - \frac{\partial \bar{\Upsilon}}{\partial \bar{\boldsymbol{\Sigma}}_F^*}\right) : \dot{\bar{\boldsymbol{\Sigma}}}_F^* + \left(\bar{\boldsymbol{H}} - \frac{\partial \bar{\Upsilon}}{\partial \bar{\boldsymbol{\Sigma}}_H^*}\right) : \dot{\bar{\boldsymbol{\Sigma}}}_H^* \\ &+ \left(J - \frac{\partial \bar{\Upsilon}}{\partial p^*}\right)\dot{p}^* + \left(\eta - \frac{\partial \bar{\Upsilon}}{\partial \theta}\right)\dot{\theta} + (\theta\dot{\eta} + \mathrm{Div}(\boldsymbol{Q}) - R)\Bigg)\,\mathrm{d}V = 0.\end{aligned} \tag{22}$$

Therein, $\boldsymbol{\pi} = \rho_0 \dot{\boldsymbol{\varphi}}$ denotes the linear momentum and $\boldsymbol{Q} = -\boldsymbol{F}^{-1}\boldsymbol{K}(\theta)\boldsymbol{F}^{-\mathrm{T}}$ is the Piola-Kirchhoff heat flux defined via the Duhamel's law. In what follows, we assume isotropic thermal material behavior and write the positive semi-definite thermal conductivity tensor as $\boldsymbol{K} = K_{\mathrm{ref}}(1 - \omega(\theta - \theta_{\mathrm{ref}}))\boldsymbol{I}$, where ω is a softening parameter. Moreover, $\boldsymbol{B}$ and R are prescribed body forces and heat sources, respectively.

Assuming that the rates of change in (22) can be chosen arbitrary, we apply suitable substitutions, namely $\dot{\boldsymbol{\varphi}} = \delta\boldsymbol{\varphi}$, $\dot{\bar{\boldsymbol{\Sigma}}}_F^* = \delta\bar{\boldsymbol{\Sigma}}_F$, $\dot{\bar{\boldsymbol{\Sigma}}}_H^* = \delta\bar{\boldsymbol{\Sigma}}_H$ and $\dot{p}^* = \delta p$ and obtain

$$\begin{aligned}G_\varphi &= \int_{\mathcal{B}_0} (\delta\boldsymbol{\varphi} \cdot \dot{\boldsymbol{\pi}} + \boldsymbol{P} : \nabla(\delta\boldsymbol{\varphi}))\mathrm{d}V - \int_{\mathcal{B}_0} \delta\boldsymbol{\varphi} \cdot \boldsymbol{B}\mathrm{d}V - \int_{\partial\mathcal{B}_0^T} \delta\boldsymbol{\varphi} \cdot \bar{\boldsymbol{T}}\mathrm{d}A = 0, \\ G_\theta &= \int_{\mathcal{B}_0} (\delta\theta\theta\dot{\eta} - \boldsymbol{Q} \cdot \nabla(\delta\theta))\mathrm{d}V - \int_{\mathcal{B}_0} \delta\theta R\mathrm{d}V - \int_{\partial\mathcal{B}_0^Q} \delta\theta\bar{Q}_{\mathrm{N}}\mathrm{d}A = 0,\end{aligned} \tag{23}$$

[3]In the following the star indicates independent variables.

supplemented by the geometric compatibility conditions

$$
\begin{aligned}
G_{\Sigma_F} &= \int_{\mathcal{B}_0} \left(\bar{\boldsymbol{F}} - \frac{\partial \bar{\Upsilon}}{\partial \bar{\boldsymbol{\Sigma}}_F^*} \right) : \delta \bar{\boldsymbol{\Sigma}}_F \mathrm{d}V = 0, \\
G_{\Sigma_H} &= \int_{\mathcal{B}_0} \left(\bar{\boldsymbol{H}} - \frac{\partial \bar{\Upsilon}}{\partial \bar{\boldsymbol{\Sigma}}_H^*} \right) : \delta \bar{\boldsymbol{\Sigma}}_H \mathrm{d}V = 0, \\
G_p &= \int_{\mathcal{B}_0} \left(J - \frac{\partial \bar{\Upsilon}}{\partial p^*} \right) \delta p \mathrm{d}V = 0.
\end{aligned}
\tag{24}
$$

Note that the thermal compatibility condition $\eta = \partial \bar{\Upsilon} / \partial \theta$ is satisfied locally.

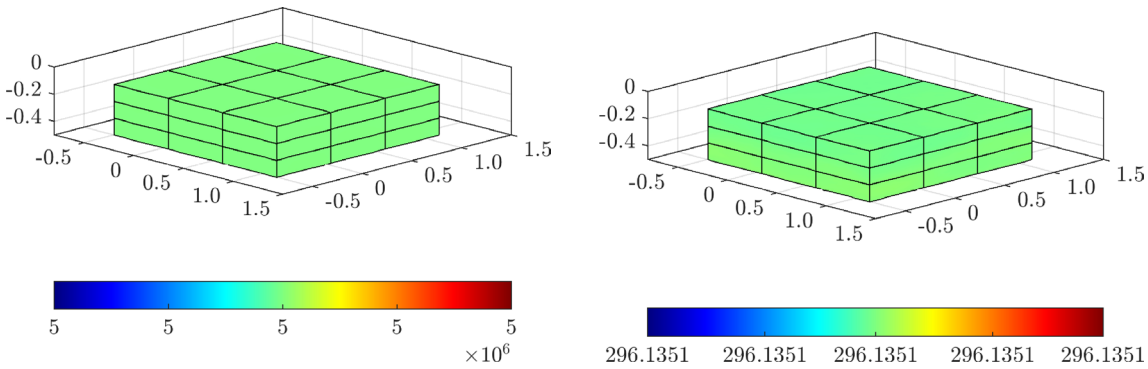

Figure 2: Patch test: Von Mises stress distribution (left) and temperature distribution (right) for the Hellinger-Reissner approach.

5 DISCRETE SETTING AND CONDENSATION

For the spatial discretization we apply a novel scheme which relies on developments suggested in Bonet et al. [5]. In particular, we utilize quadratic finite element based shape functions for the spatial discretization of the geometry and the temperature, whereas element wise linear interpolations are applied to the conjugate stresses such that we can apply a condensation procedure to eliminate this stress unknowns within the global system, see Dittmann [6] for more details. Furthermore, an implicit time integration scheme is applied to the semi-discrete coupled thermoelastic problem to obtain a set of non-linear algebraic equations to be solved via the Newton-Raphson iteration scheme. Eventually, the global system to be solved within each Newton-Raphson iteration reads

$$
\begin{bmatrix}
\boldsymbol{K}_{\varphi\varphi} & \boldsymbol{K}_{\varphi\theta} & \boldsymbol{K}_{\varphi\Sigma} \\
\boldsymbol{K}_{\theta\varphi} & \boldsymbol{K}_{\theta\theta} & \boldsymbol{K}_{\theta\Sigma} \\
\boldsymbol{K}_{\Sigma\varphi} & \boldsymbol{K}_{\Sigma\theta} & \boldsymbol{K}_{\Sigma\Sigma}
\end{bmatrix}
\begin{bmatrix}
\Delta \boldsymbol{q} \\
\Delta \boldsymbol{\Theta} \\
\Delta \boldsymbol{\Sigma}
\end{bmatrix}
=
\begin{bmatrix}
\boldsymbol{R}_{\varphi} \\
\boldsymbol{R}_{\theta} \\
\boldsymbol{R}_{\Sigma}
\end{bmatrix},
\tag{25}
$$

where $\Delta \boldsymbol{q} = [\Delta \boldsymbol{q}_1, \dots, \Delta \boldsymbol{q}_N]$ and $\Delta \boldsymbol{\Theta} = [\Delta \Theta_1, \dots, \Delta \Theta_N]$ represent the incremental variations of the nodal values of the displacement field and the temperature field at the current time step. Moreover, $\Delta \boldsymbol{\Sigma} = [\Delta \bar{\boldsymbol{\Sigma}}_{F,1}, \dots, \Delta \bar{\boldsymbol{\Sigma}}_{F,n}, \Delta \bar{\boldsymbol{\Sigma}}_{H,1}, \dots, \Delta \bar{\boldsymbol{\Sigma}}_{H,n}, \Delta p_1, \dots, \Delta p_n]$ summarizes the incremental variations of the element wise nodal values of the conjugate stress fields.

Solving (25) with respect to $\Delta \boldsymbol{\Sigma}$ yields

$$\Delta \boldsymbol{\Sigma} = \boldsymbol{K}_{\Sigma\Sigma}{}^{-1} (\boldsymbol{R}_\Sigma - \boldsymbol{K}_{\Sigma\varphi} \Delta \boldsymbol{q} - \boldsymbol{K}_{\Sigma\theta} \Delta \boldsymbol{\Theta}) \tag{26}$$

and insertion into (25) gives us the condensed system

$$\begin{bmatrix} \boldsymbol{K}_{\varphi\varphi} - \boldsymbol{K}_{\varphi\Sigma} \boldsymbol{K}_{\Sigma\Sigma}^{-1} \boldsymbol{K}_{\Sigma\varphi} & -\boldsymbol{K}_{\varphi\Sigma} \boldsymbol{K}_{\Sigma\Sigma}^{-1} \boldsymbol{K}_{\Sigma\theta} \\ -\boldsymbol{K}_{\theta\Sigma} \boldsymbol{K}_{\Sigma\Sigma}^{-1} \boldsymbol{K}_{\Sigma\varphi} & \boldsymbol{K}_{\theta\theta} - \boldsymbol{K}_{\theta\Sigma} \boldsymbol{K}_{\Sigma\Sigma}^{-1} \boldsymbol{K}_{\Sigma\theta} \end{bmatrix} \begin{bmatrix} \Delta \boldsymbol{q} \\ \Delta \boldsymbol{\Theta} \end{bmatrix} = \begin{bmatrix} \boldsymbol{R}_\varphi - \boldsymbol{K}_{\varphi\Sigma} \boldsymbol{K}_{\Sigma\Sigma}{}^{-1} \boldsymbol{R}_\Sigma \\ \boldsymbol{R}_\theta - \boldsymbol{K}_{\theta\Sigma} \boldsymbol{K}_{\Sigma\Sigma}{}^{-1} \boldsymbol{R}_\Sigma \end{bmatrix} \tag{27}$$

to be solved with respect to $\Delta \boldsymbol{q}$ and $\Delta \boldsymbol{\Theta}$. In a last step, (26) can be used to obtain the stress update $\Delta \boldsymbol{\Sigma}$.

6 NUMERICAL EXAMPLES

In this section we present quasi-static as well as transient examples to demonstrate the applicability and performance of the Hellinger-Reissner type variational principle for fully coupled non-linear thermoelasticity.

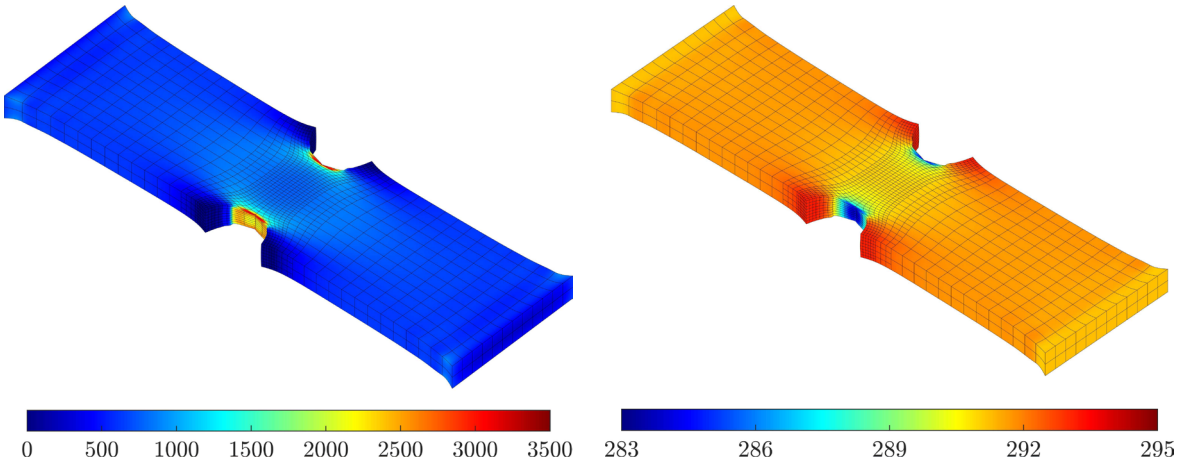

Figure 3: Notched bar: Von Mises stress distribution (left) and temperature distribution (right). Results for a displacement of $u = 3$ using the Hellinger-Reissner approach and the refined mesh are depicted.

6.1 Patch test

We start with a quasi-static patch test example to demonstrate the applicability of the Hellinger-Reissner approach. Here, we consider a block of size $0.5 \times 0.5 \times 0.5$ where

a uniform pressure load of $p = 5 \times 10^6$ is applied. The mechanical parameters for the Mooney-Rivlin material law are given by $\alpha = 15/13 \times 10^5$,$\beta = 10/13 \times 10^5$ and $\kappa = 25/3 \times 10^5$, which correspond to a Young's modulus of $E = 10^6$ and to a Poisson's ratio of $\nu = 0.3$. Moreover, the parameters for the thermal material behavior are specified by $c = 1830$, $\gamma = 0.22333$ and $K = K_{\text{ref}} = 0.55$. The initial temperature is set to 293.15.

Figure 2 shows nearly perfect and uniform results for the von Mises stress distribution and temperature distribution after loading. Therein, the color map for the von Mises stress distribution is in range of $5 \times 10^6 \pm 10^{-5}$, whereas a range wide of $\pm 2 \times 10^{-11}$ is used for the temperature distribution.

6.2 Notched bar

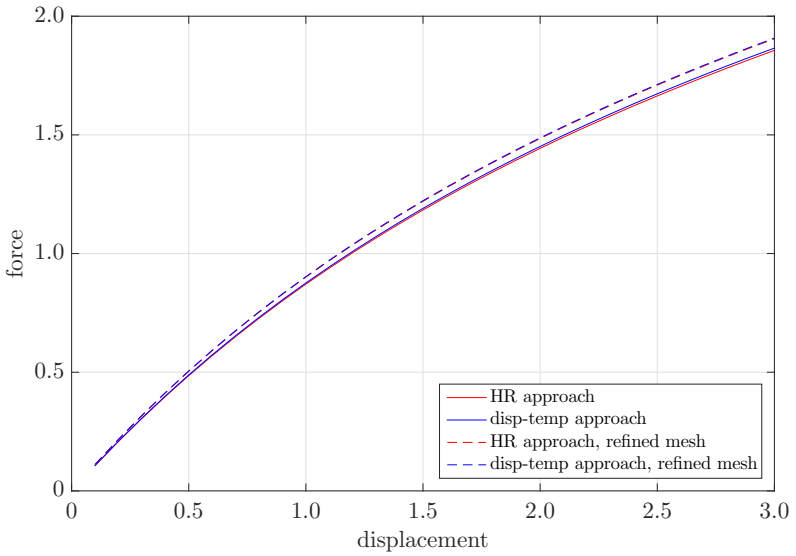

Figure 4: Notched bar: Load-deflection curves for the Hellinger-Reissner and the displacement-temperature based approach using the unrefined as well as the refined mesh.

Next, we consider a further quasi-static example to investigate the convergence of the Hellinger-Reissner approach in comparison to the displacement-temperature based approach. In particular, the ends of a notched rectangular bar of size $10 \times 4.8 \times 1$ are moved apart until an increase of length of approximately 60 percent is achieved, see Hesch & Betsch [9] and Holzapfel and Simo [2] for more details. The Mooney-Rivlin material parameters are given as follows, for the mechanical field the parameters take the values $\alpha = 1500/13$, $\beta = 1000/13$ and $\kappa = 2500/3$, whereas the setting for the thermal field reads $\theta_0 = 293.15$, $c = 1830$, $\gamma = 2.2333 \times 10^{-2}$ and $K = K_{\text{ref}} = 0.55$. The corresponding Young's modulus is given by $E = 1000$ and the Poisson's ratio by $\nu = 0.3$. For the numerical simulations, a mesh consisting of $32 \times 12 \times 2$ elements with 5936 thermal and

mechanical degrees of freedom is used as well as a locally refined mesh consisting of overall 5808 elements with in total 18982 degrees of freedom.

Figure 3 shows the von Mises stress distribution and temperature distribution of the deformed geometry. Eventually, the load-deflection curve is plotted in Figure 4 for the Hellinger-Reissner as well as the displacement-temperature based approach and both meshes. For both approaches nearly identical results are obtained.

6.3 L-shaped block

Eventually, we deal with a transient thermoelastic problem consisting a L-shape block of size $2.4 \times 1.2 \times 3.6$, see also Hesch & Betsch [9]. The L-shape is discretized by 1012 elements with overall 6792 thermal and mechanical degrees of freedom. Additionally, a local refinement is applied to the region where we expect peak stresses due to the notch of the L-shape. The Mooney-Rivlin material parameters are given by $\alpha = 114.9425$, $\beta = 57.4713$ and $\kappa = 3333.3333$, which correspond to a Young's modulus of $E = 1000$ and to a Poisson's ratio of $\nu = 0.45$. The mass density is set to $\rho = 0.5$. Moreover, the thermal material setting reads $\theta_0 = 293.15$, $c = 1830$, $\gamma = 2.2333 \cdot 10^{-4}$ and $K_{\text{ref}} = 0.15$ with $\omega = 0.004$. The body is subjected to a temporal traction load $p(t) = p_{\max} \sin(\pi t)$ during the time interval $t \in [0, 1]$ with a peak load of $p_{\max} = 60$. Afterwards, the body moves freely in space for the time interval $t \in [1, 5]$.

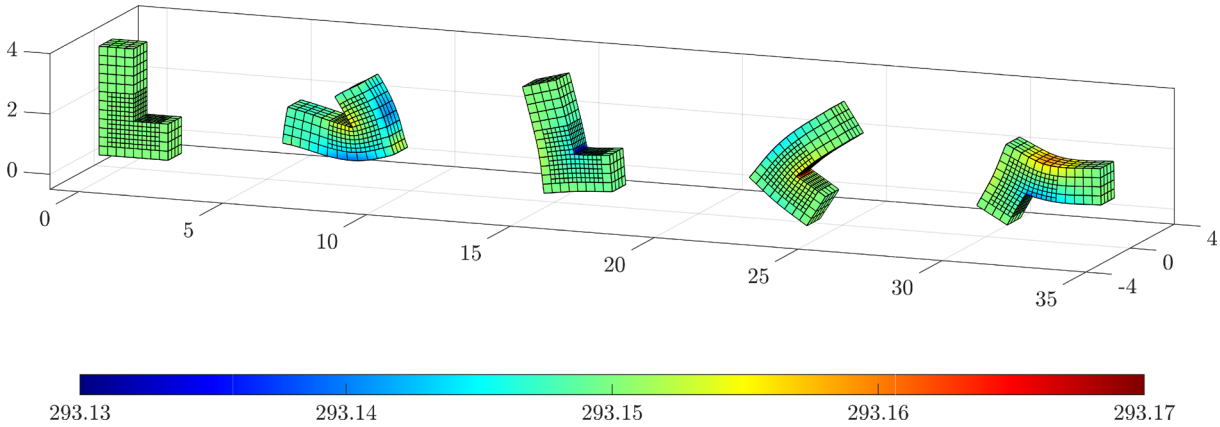

Figure 5: L-shaped block: Snapshots of the deformed configuration at times $t = [0, 0.46, 0.71, 0.96, 1.21]$.

The motion of the body and the associated temperature distribution is illustrated in Figure 5 using a time step size of $\Delta t = 0.01$. For both, the Hellinger-Reissner as well as the displacement-temperature based approach, the applied time step size used in combination with a standard mid-point type time integration scheme is sufficiently small to keep changes in the total energy small enough such that the convergence is not affected, see Figure 6. More advanced energy consistent time integration schemes for

non-linear thermoelasticity can be found in Hesch and Betsch [9] and Dittmann et al. [10]. Additionally, the angular momentum is plotted over time in Figure 6. As expected, the components of angular momentum remain preserved for the considered problem and time integration scheme.

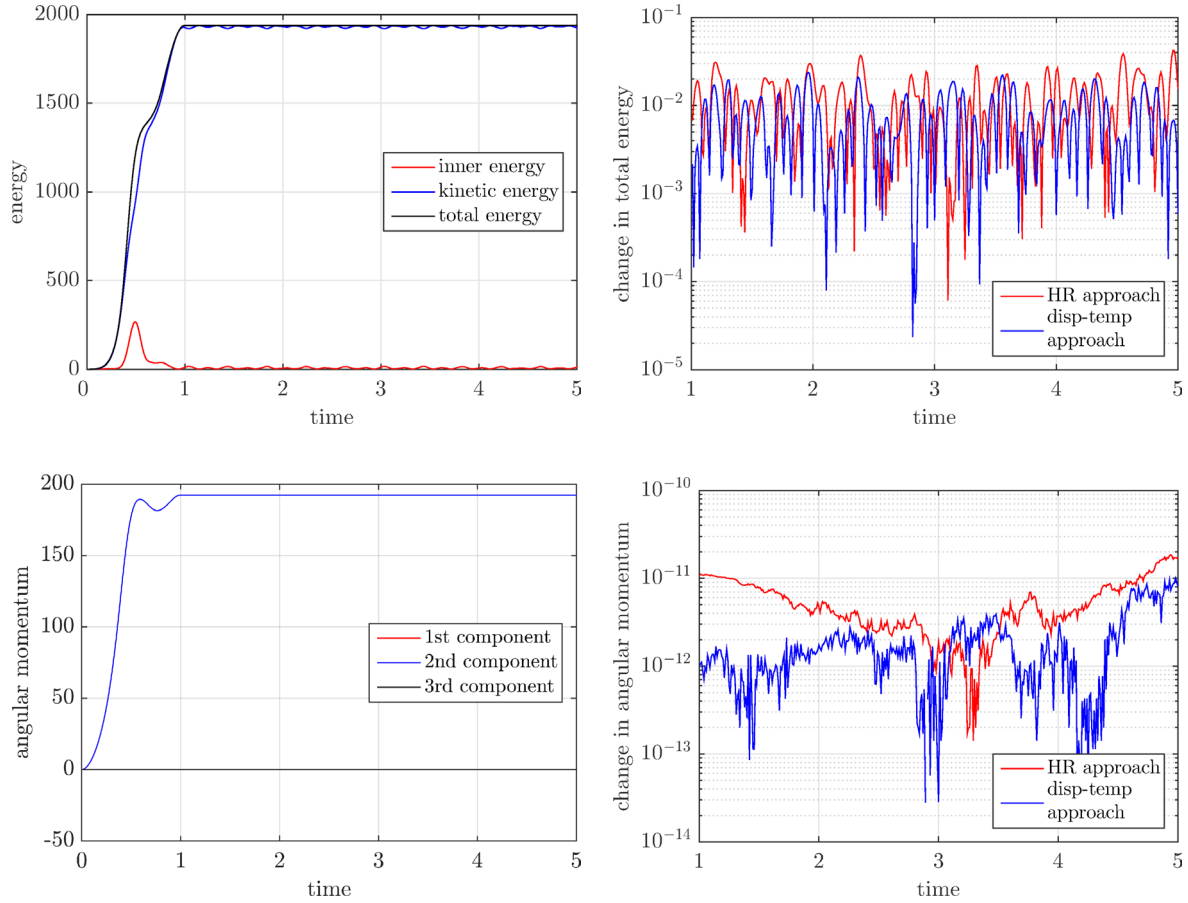

Figure 6: L-shaped block: Energy and angular momentum plotted over time.

7 CONCLUSIONS

In the present work a novel formulation based on a mixed Hellinger-Reissner type variational principle has been applied to large strain thermomechanical coupled problems. A series of computational simulations has demonstrated the applicability and performance of this approach in comparison to standard displacement-temperature based formulations. The numerical results has been shown to be in accordance with the displacement based solution in terms of accuracy and convergence. Thus, the proposed Hellinger-Reissner type variational principle represents a novel and alternative formulation, which provides high

flexibility and simplicity for the modeling of multi-field problems due to the additional primal fields, see also Hesch et al. [7]. Moreover, the construction of the discretization allows for the application of a condensation procedure such that no significant increase of computational effort has been emerged.

REFERENCES

[1] Reese, S. and Govindjee, S. Theoretical and Numerical Aspects in the Thermo-Viscoelastic Material Behaviour of Rubber-Like Polymers. *Mechanics of Time-Dependent Materials* (1997) **1**(4):357–396.

[2] Holzapfel, G.A. and Simo, J.C. Entropy elasticity of isotropic rubber-like solids at finite strains. *Computer Methods in Applied Mechanics and Engineering* (1996) **132**(1):17–44.

[3] Miehe, C. Entropic thermoelasticity at finite strains. Aspects of the formulation and numerical implementation. *Computer Methods in Applied Mechanics and Engineering* (1995) **120**(3–4):243–269.

[4] Ball, J. Convexity conditions and existence theorems in nonlinear elasticity. *Archive for Rational Mechanics and Analysis* (1976) **63**:337–403.

[5] Bonet, J., Gil, A.J. and Ortigosa, R. A computational framework for polyconvex large strain elasticity. *Computer Methods in Applied Mechanics and Engineering.* (2015) **283**:1061–1094.

[6] Dittmann, M. *Isogeometric analysis and hierarchical refinement for multi-field contact problems*. PhD thesis (2017) doi: 10.5445/KSP/1000063914.

[7] Hesch, C. and Gil, A.J. and Ortigosa, R. and Dittmann, M. and Bilgen, C. and Betsch, P. and Franke, M. and Janz, A. and Weinberg, K. A framework for polyconvex large strain phase-field methods to fracture. *Computer Methods in Applied Mechanics and Engineering* (2017) **317**:649–683.

[8] de Boer, R. *Vektor- und Tensorrechnung für Ingenieure*. Springer-Verlag Berlin, Heidelberg, (1982).

[9] Hesch, C. and Betsch, P. Energy-momentum consistent algorithms for dynamic thermomechanical problems—Application to mortar domain decomposition problems. *International Journal for Numerical Methods in Engineering* (2011) **86**(11):1277–1302.

[10] Dittmann, M., Franke, M., Temizer, İ. and Hesch, C. Isogeometric Analysis and thermomechanical Mortar contact problems. *Computer Methods in Applied Mechanics and Engineering* (2014) **274**:192–212.